Title: A heat-pulse method for detecting ice formation on surfaces

Authors: Patrice D. Dongo[1], Hatim Machrafi[2], C. Minetti[1], Alessandro Amato[1], P.Queeckers[1], C.S. Iorio[1*]

[1]Microgravity Research Centre, Université libre de Bruxelles, Campus Solbosch, CP165/62, Avenue P.Héger, 1050, Brussels, Belgium,
[2] Thermodynamics of Irreversible Phenomena, Université de Liège, Allée du 6-Août, 19, 4000 Belgium
[*] E-mail: ciorio@ulb.ac.be

Abstract
Early detection of ice formation on surfaces is a crucial requirement in many applications such as wind turbines, aeroplane's wings, radar domes. This paper presents the concept of a heat-pulse ice detection system. Its principle consists of recording the temperature evolution and assessing the relaxation time after the surfaces are subject to a heat excitation generated by an electrical pulse. The sensor comprises thin graphene films embedded in pre-preg layers of aeronautical grade as well as thermocouples to record the temperatures profiles at given locations. The criterium of ice detection exploits the high thermal capacity of ice compared to the air to capture the formation of icy spots. Numerical simulations and comparison with experimental investigations have been carried out to validate the principle and criteria of the ice detection system. [aggiungere ultima frase]
Keywords: Ice detection criteria, ice thermal capacity, graphene, heat-pulse, ice formation, thermal relaxation, thermal excitation

1. Introduction

Detection of ice is relevant and very important in several domains like wind energy [1-2], road, maritime and air traffic [3]. The appearance of ice requires particular environmental conditions (ambient temperature, moisture, airspeed) and is an issue especially for aerial transport. In fact, in air traffic, during the flight when the temperature, associated at this phenomenon, is comprised between -40°C and 0°C, ice forms from supercooled water droplets that come from clouds at moist air conditions [4-6]. Depending on the environmental conditions, such as moisture, ambient temperature, airflow speed, ice accretion could be classified as glazed, rime and mixed. Glazed ice, also called clear ice, is formed in the clouds at relatively high temperatures with large water droplets [7]. Rime ice appears when the temperatures are low, and the droplets are small, while mixed ice is the result of a combination of clear and rime ice due to a spatial variation of clouds [8-9]. Accumulation of ice on wings, slats, and rudders of an aeroplane affects its aerodynamic performance significantly, increases the drag force and reduces the capacity of the aircraft to create lift, dramatically [10-11].
Furthermore, ice accretion affects the communication and localisation of a plane negatively and can cause severe accidents. Icing accretion on wings and tail have been reported to be responsible for 10% of fatal aircraft accidents [12]. Several approaches, technologies and methods have been proposed and implemented by researchers and companies to overcome ice formation and its consequences. The majority of these de-icing devices are developed with the physical principle of vibration and are based mostly on optical, mechanical, electrical and combined modes of transduction [13-16]. Many of these existing sensors nowadays are costly, requiring significant constraints of implementation and maintenance. Furthermore, during the de-icing process, substantial quantity and the unnecessary energy consumption is required for the heating of the non-frozen area of the wings of an aeroplane. Among the several approaches, to the best of our knowledge, none really exploit the thermal properties of ice to assure its detection.

This paper presents a method to detect the formation of ice. This approach uses a temperature feedback reading induced by a heat pulse, a technique based on the exploitation of the thermal capacity of ice. The sensor devices that are developed under these approaches are of the low–cost type, with a good sensitivity, including the capability to detect and counteract in real time the formation of ice exactly where it appears. Furthermore, it also allows for eliminating the ice spots in an energy-efficient way.

2. Experimental setup and procedure

The experimental setup is sketched in Fig.1.It consists of two main blocks: the control and acquisition unit (CAU) and the test cell. The control and acquisition unit comprises a DC power supply (TTi EL302P, 30V, 2A), a relay card, T type thermocouples, dedicated software for creating a pulse shaped signal, and data logger (Agilent 34970A) - Fig.1 (a),(b),(c),(f). Substrates are in Fibre Glast Pre-Preg composite. Pre-preg is the collective term for a reinforcing fabric which has been pre-impregnated with a resin system, typically epoxy of the class used in the aeronautical sector. They embed graphene ribbons used as heating elements and thermocouples. The test cells are assembled, starting from two non-cured Pre-Preg layers. Graphene ribbons (Nanesa GS-50, electrically conductive, 5Ohm) with size 40mm x 5mm x 0.05mm and T type thermocouples are inserted between the two layers as well as the thin -foil electrical contacts. The composite layers are then pressed to eliminate any air bubble and cured in an oven at 150 °C during 3 hours. The cured cells are shown in Fig.1 (e). During the experiments, the test cells are enclosed in a home-made environmental chamber where temperature and humidity are controlled. Typical values range for temperature and humidity are -30°C± 1°C and 32% ± 2%, respectively. A set of Peltier elements and a thermal bath loop are used for cooling down the test cells - Fig.1 (d).

The working principle of the method consists in sending through the computer-controlled relay card short electrical pulses through the graphene-ribbons embedded in the substrates on which ice droplets are formed to generate successive pulsed heating by Joule heating effect. Thermocouples detect the temperature variation at a different spot on the test cells. The temperature timeline is recorded thanks to the data-logger. The time required for the excited region of the test cell to return to its initial temperature as well as the shape of the temperature signals are analysed. The experiments were performed by depositing droplets of different water volumes right on top or close to the position of the thermocouples in the substrate.

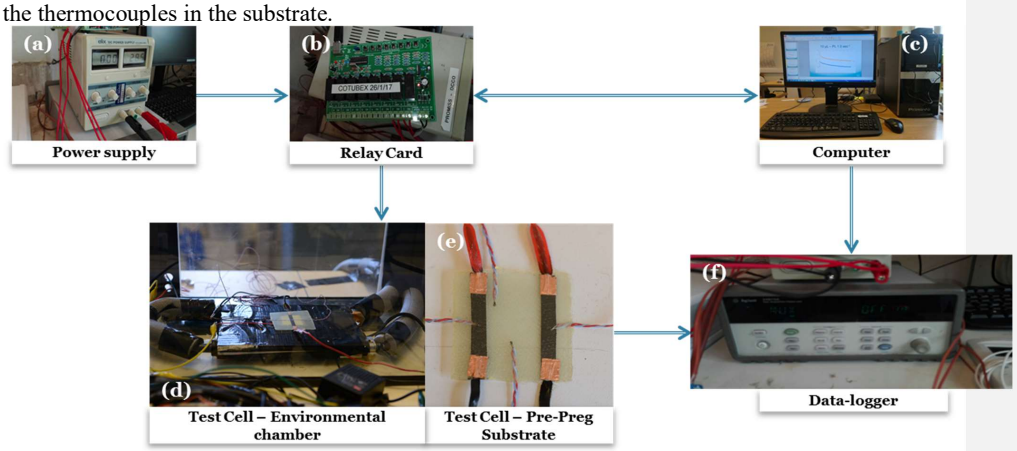

Fig. 1 Sketch of the experimental setup: (a) DC supply, (b) relay, (c) computer, (d) Environmental chamber , (e) Pre-Peg, embedding graphene layers and thermocouples, (f) datalogger

3. Numerical model

To better understand the experiments, a numerical model has been constructed using COMSOL Multiphysics with the geometry given in Fig. 2. It includes the different domains in the setup: air, ice and substrate. This model simulates the experiment, applying an electrical pulse through the graphene sheet ~~1~~, which causes the temperature to increase due to the Joule effect. The shape of the ice is considered semi-spherical. The physics used are heat transfer in solids and fluids in the transient state.

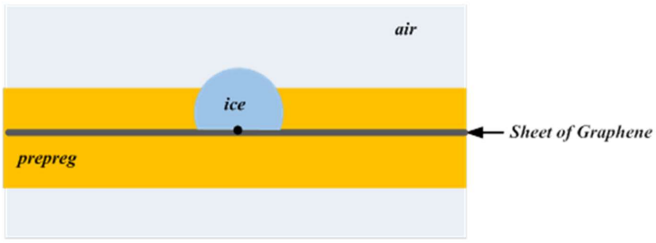

Fig.2. COMSOL 2D model of the active method with ice

In order to give the comparison a quantitative character, three sample points are considered, as shown in Fig. 3, which correspond geometrically to the ones present in the experimental setup. This will also allow to assess the ability of the numerical model to follow correctly the heat transfer through the different materials. This is important if we would like to use this model for further physical interpretation as will be proposed later. ~~To have a better comparison with the experimental setup, three sample points have been considered, as shown by Fig. 3.~~

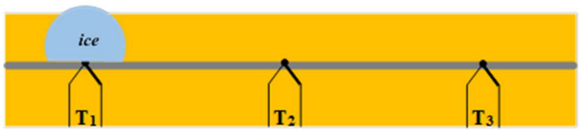

Fig.3. Sample points in COMSOL showing thermocouples positioning

The energy balance for a phase *i* is generally given by:

$$\rho_i C_{pi} \frac{\partial T_i}{\partial t} + \rho_i C_{pi} \boldsymbol{u} \cdot \nabla \mathrm{T}_i + \nabla \cdot (\lambda_i \nabla T_i) = \mathrm{Q} + \mathrm{Q}_{ted} \qquad (1)$$

Where Q, Q_{ted}, ~~,~~t and $\boldsymbol{u}$ are the heat source, thermoelastic damping, time and local velocity field respectively. Furthermore, T_i, ρ_i, C_{pi} and λ_i are the temperature, density, heat capacity and thermal conductivity of the phase denoted by the subscript i. As the experimental tests have been carried out in the fridge with weak airflow, we can neglect convection, so we assume $\boldsymbol{u} = 0$ ~~,~~in Eq. (1). This assumption will be justified later. To deliver heat with a specific specified electrical pulse duration, the mathematical expression for the Joule heating function used is given by the following expression.

Formatted: Font: Not Bold

$$P_j(t) = \begin{cases} RI^2 \ if \ \ t_i < t < t_f \\ 0 \quad otherwise \end{cases} \qquad (2)$$

$t_f - t_i$, I are the pulse duration of heat source and intensity of electrical current applied to generate heat. Note that Eq. (1) should be understood in the sense that the heat source and the thermoelastic damping terms are only present in the graphene sheet. Then, R is the electrical resistance of the sheet of graphene determined with the four-probe measurement technique. ~~As the experimental tests have~~

~~been carried out in the fridge with weak airflow, we can neglect convection, so we assume $\boldsymbol{u} = 0$.~~
Continuity of the heat flux is considered at the boundaries between the substrate, ice and air:

$$q_n = q_m \qquad (3)$$

where the subscript n and m denote adjacent phases or materials. The outer boundaries are assumed to be far away from the heat source and the ice drop to experience any change, so that a constant temperature $T_0 = 243{,}15\ ^{o}K = -30\ ^{\circ}C$ can be assumed, corresponding to the initial one, which is the set temperature in the fridge. Based on this model, simulations using finite elements, are performed, where the time dependence response of the temperature after application of the electrical pulse on the substrate is measured. To validate the numerical accuracy of this model, the convergence of the results ~~have~~ has been carried out considering different mesh sizes, and the relative error ε is assessed with the following expression.

$$\varepsilon\,(\bar{x}, \bar{y},\ \mathrm{t}) = \left|\frac{T_{mesh1}(\bar{x},\bar{y},\mathrm{t}) - T_{mesh2}(\bar{x},\bar{y},\mathrm{t})}{T_{mesh1}(\bar{x},\bar{y},\mathrm{t})}\right| \qquad (4)$$

As an example, Fig. 4 shows the geometry at two mesh sizes, one with a maximum element size of 0.2 mm ~~(named normal)~~ and another of 0.1 mm ~~(named finer)~~.

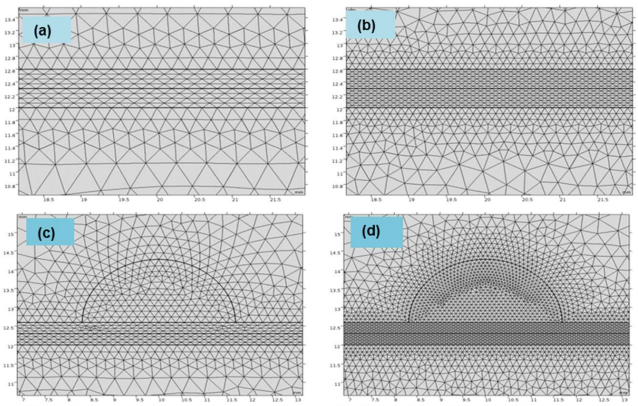

Fig.4. Representative mesh sizes (a) normal without ice; (b) finer without ice; (c) normal with ice; (d) finer with ice.

The results of the convergence tests will be discussed in the next section.

4. Results and discussions

The convergence tests are performed for the condition without ice and for three temperatures corresponding to the ones measured by the three thermocouples. The results are put in Fig. 5 next to the corresponding temperature curves. It shows that the error between the two mesh sizes was of the order of $O(10^{-5})$. ~~The numerical results given in Fig. 5 (a),(c),(e) are beforehand tested for their convergence.~~ Fig. 5 (b),(d),(f) show the curves of the relative errors $\varepsilon(T_1)$, $\varepsilon(T_2)$ and $\varepsilon(T_3)$, confirming a good convergence of the numerical model. Therefore, we consider that a maximum mesh size of 0.2 mm is sufficient for numerical accuracy and this mesh size will be used for our further investigations. As ~~mentioned~~ described before in the experimental section, tests have been done on different spots of the sensitive element (where the thermocouples are inserted in the substrate) in presence of ice and without ice. Numerical simulations are performed using the same parameters as

Formatted: Font: Not Bold, English (United States)

Formatted: English (United States)

Formatted: Font: Italic

Formatted: Font: Italic

Formatted: Font: (Default) Times New Roman, 12 pt

the experiments, followed by a comparison between the numerical and experimental results. The material properties used for numerical simulations are reported in the Table 1.

Air • **Density : ρ_{air}= 1.2Kg/m^3** • **Heat capacity: $C_{p,\,air}$ =1000 J/Kg.°K** • **Thermal conductivity : λ_{air} = 0.022W/m°K** **Graphene Ribbons** • **Density : ρ_{gr}= 1200 Kg/m^3** • **Heat capacity : $C_{p,\,gr}$ =800 J/Kg.°K** • **Thermal conductivity : λ_{gr} = 500W/m°K** • **Electrical resistance : R =0.6 Ω**	**Ice** • **Density : ρ_{ice}= 917Kg/m^3** • **Heat capacity : $C_{p,\,ice}$ =2108 J/Kg.°K** • **Thermal conductivity : λ_{ice} = 2.5W/m°K** **Pre-Preg** • **Density : ρ_{pp}= 2000Kg/m^3** • **Heat capacity : $C_{p,\,pp}$ =860 J/Kg.°K** • **Thermal conductivity : λ_{pp} = 0.25W/m°K**

Table 1 Material properties

~~The experiments are compared with the numerical simulations. According to numerical and experimental considerations~~The experimental results without ice are shown in Fig. 5, accompanied by the corresponding numerical results for the temperatures measured at the aforementioned three thermocouples, i.e. ~~some results corresponding to the thermal response of thermocouples~~ $T_1(t)$, $T_2(t)$ and $T_3(t)$. ~~–~~The numerical results given in Fig. 5 (a),(c),(e) are beforehand tested for their convergence. ~~without ice and relative errors curve (c) for each case are given by Fig.5.~~ These results are the superposition of numerical and experimental tests after application through the graphene sheet of an electrical pulse of a duration of Δt_{pulse} =5s and a power of P = 1.15W.

Formatted: Font: (Default) Times New Roman, 12 pt

Formatted: Normal

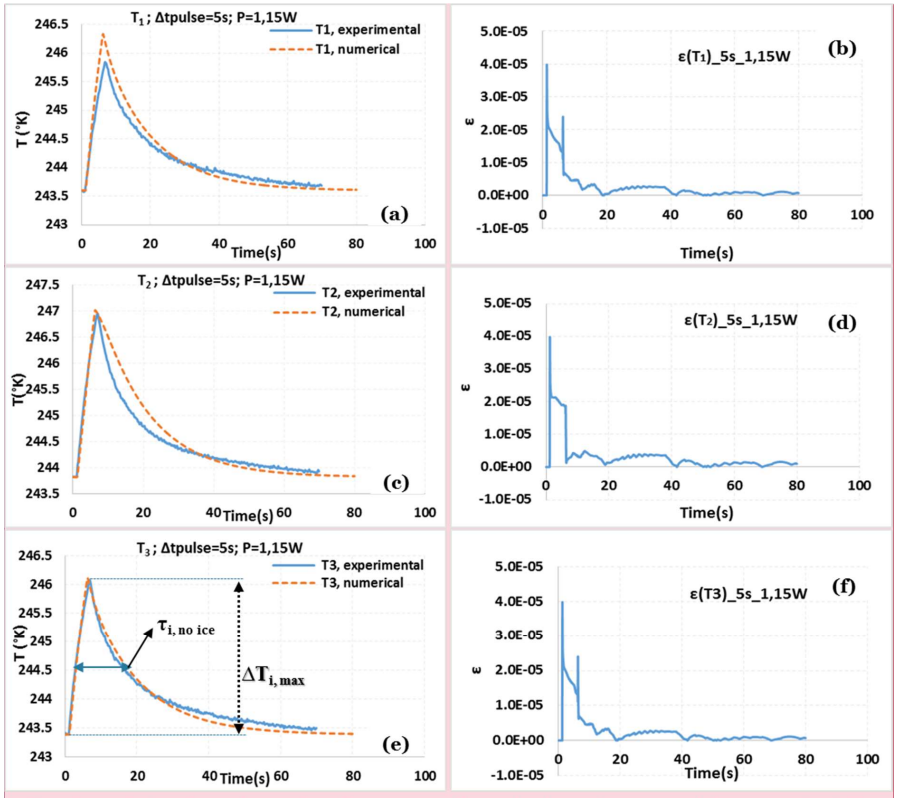

Fig.5 Numerical and experimental results corresponding to the thermal response of thermocouples $T_1(t)$, $T_2(t)$ and $T_3(t)$ without ice and relative errors curve (ε)

$\Delta T_{i,\,max}$ and $\tau_{i,\,no\ ice}$ represent respectively the maximum of the temperature response of thermocouple and the time duration between two successive values of the temperature equal to 50 % of $\Delta T_{i,\,max}$, whereas the subscript i denotes the thermocouple considered. The table below gives the values of these ~~parameters~~ results ~~for the results given~~ in Fig.5. We can see a rather good comparison between the numerical values and the experimentally measured ones. This allows the analysis of the results that follow, where the cases with ice deposition are considered.

Table 2 Numerical and experimental comparison of representative ~~parameters~~ results given by temperature profile of thermocouples T_1, T_2 and T_3

Parameters	Numerical	Experimental	Relative Error
$\Delta T_{1,max}$	2.7 °K	2.6 °K	0.1716
$\tau_{1,\,no\ ice}$	10.57 s	10.45 s	0.0328
$\Delta T_{2,max}$	3.19 °K	3.12 °K	0.0239
$\tau_{2,\,no\ ice}$	12 s	10s	0.2879
$\Delta T_{3,max}$	2.6 °K	2.61 °K	0.0133
$\tau_{3,\,no\ ice}$	10.43 s	10.37 s	0.1083

Commented [U1]: Il faut vraiment améliorer le format des figures : pas de quadrillages, figure caption ne dot pas être inclus dans l'images, mais écrit explicitement dans le texte

~~The numerical results given in Fig. 5 (a),(c),(e) are beforehand tested for their convergence. Fig. 5 (b),(d),(f) show the curves of the relative errors $\varepsilon(T_1)$, $\varepsilon(T_2)$ and $\varepsilon(T_3)$, confirming a good convergence of the numerical model.~~

Considering thermocouple T_1, experimental tests and numerical simulations have been done for different volumes (10µl, 40µl, 80µl) of ice-drops and compared with the case without ice. The results are reported in Fig.6.

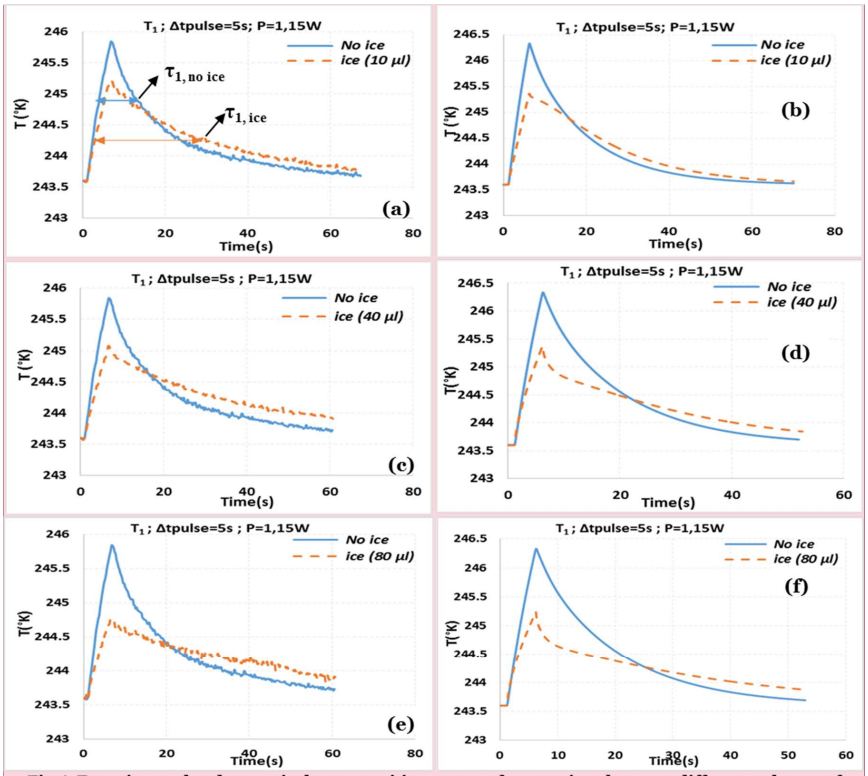

Fig.6. Experimental and numerical superposition curves of comparison between different volumes of ice and without ice for T_1. (a) experimental between 10µl and without ice, (b) numerical between 10µl and without ice, (c) experimental between 40µl and without ice, (d) Numerical between 40µl and without ice, (e) experimental between 80µl and without ice, (f) numerical between 80µl and without ice.

The experimental and numerical results for the cases with ice deposition show an agreement in temperature profiles. To asses quantitatively this comparison, the values $\Delta T_{1,\,max}$ and τ_1 are presented in Table 3 for the cases with and without ice for thermocouple number 1. It shows that the values are close to one another. It also shows that for both the cases with and without ice the numerical model corroborates the experimental criterion quite well, which reinforces the argument that such a criterion could well be used for ice-detection. Indeed, we clearly see that the values of $\Delta T_{1,\,max}$ and τ_1 change significantly when ice is present with regards to the case without ice. Both the experimental values and the numerical results confirm this finding. We can therefore propose ~~It clearly appears~~ from the

Commented [U2]: Même chose, améliorer les figures et aussi mettre les échelle aux même valuers entre, p.ex. 242 et 247 K.

results given in Fig.6.a that the representative parameters $\Delta T_{1,\,max}$ and $\tau_{1,}$ of which the values are reported in table 3, can be used ~~like~~ as reliable criteria for ice detection.

Table 3. Numerical and experimental values of the temperature response (using the temperature profile T_1) and relaxation time for the cases with a 10µl ice-drop and without an ice-drop.

Parameters	Numerical	Experimental
$\Delta T_{1,max\_no\ ice}$	2.7 °K	2.6 °K
$\tau_{1,\,no\ ice}$	10.57 s	10.45 s
$\Delta T_{1,max\_ice}$	1.75 °K	1.63 °K
$\tau_{1,\,ice}$	20.4 s	19.5 s

Table 3 shows that $\tau_{1,\,ice} \approx \mathbf{2}\,\tau_{1,\,no\ ice}$ and $\Delta T_{1,\,max\_no\ ice} > \Delta T_{1,\,max\_ice}$.

Let us look more in detail In fact, according to the fact that tests have been carried out under a surrounding temperature of 243°K, the no-ice condition represents the presence of air. The results show clearly that the temperature increase, induced by the electrical pulse, is lower when ice is present, with a higher relaxation time. ~~Based on the results obtained, observation is that~~ Knowing that ice ~~behaves like~~has a larger thermal capacitance, ~~having a capacity to~~ storinge more energy, than ~~compared to~~ air, the presence of ice is tantamount to a more delayed temperature response and heat dissipation. This assertion is strongly sustained by the fact that density and heat capacity of ice are greater compared to the ones of air. For instance, let us consider the density and heat capacity of the material~~, respectively~~. Then, for the same volume of the material V, the evaluation of thermal capacitance $C_{th,j}$ is given by:

$$C_{th,j} = \rho_j \,.\, c_j \,.\, V \qquad (5)$$

where ~~Where~~ j can ~~define~~ stands either for ice or air. It is then interesting to translate this thermal process in an equivalent electrical circuit, represented in a simplified manner by Fig. 7.

~~Experimental process of this work can be simplified by Fig.7, which helps to understand the working principle of the active method.~~

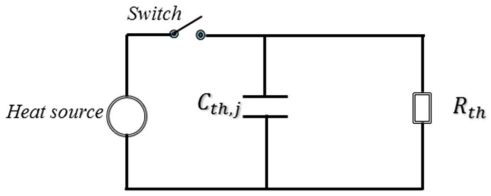

Fig.7. Equivalent electrical diagram of the system of ice detection

~~The switch is closed~~ Wwhen the electrical pulse is applied, this corresponds to a closed switch, leading to the generated ~~and~~ heat ~~generated is~~being stored in the thermal capacitor $C_{th,j}$, which could be ice or air. Moreover, R_{th} is the global resistance taking into account the thermal resistance of air and the substrate in which the accumulated heat ~~accumulated~~ is dissipated. As the thermal conductivity of air is too low compared to that of the substrate, the heat stored by the ice is assumed to be primarily released to the substrate, neglecting any dissipation to the air. In order to assess the

Commented [U3]: Tu n'as pas les même valeurs manips et numérique pour les autres 2 thermocouples ? Ce serait intéressant de juste les ajouter dans le tableau et voir est-ce que cela montre la même tendance ou pas…

Commented [U4]: Ce serait aussi intéressant d'utiliser le modèle pour reproduire des valeurs comm dans le tableau 3 avec d'autre température d'air et autre taille de glace pour encore renforcer le critère.. Je pense que ceci serait important pour faire valoir le critère. C'est ce que je dirais, si j'étais référé.

Formatted: Font: Bold

degree of importance of heat convection with respect to heat conduction for our setup, we define a Biot number as~~Based on the experimental and numerical data, evaluation of the Biot number *Bi* (~~ the ratio of the conductive heat resistance within the object to the convective heat transfer resistance across the body's boundary.)~~ The Biot number *Bi* is then given by relation (6):

$$Bi = \frac{h_j(V_j/A_j)}{\lambda_j} \qquad (6)$$

where h_j, V_j, A_j and λ_j are respectively heat transfer coefficient around the body, volume, surface and thermal conductivity of the body. The Biot numbers has been calculated from the ~~obtained from~~ experimental measurements and the numerical simulations for ice drop volumes of 10, 40, 80 and 100µl ~~of ice drop considered and~~ positioned on thermocouple T_1 ~~for~~corresponding to an electrical pulse of 1.15 W with a duration of 5s~~, of duration of electrical pulse of 1.15W are reported on Fig.8.~~ The results are shown in Fig. 8.

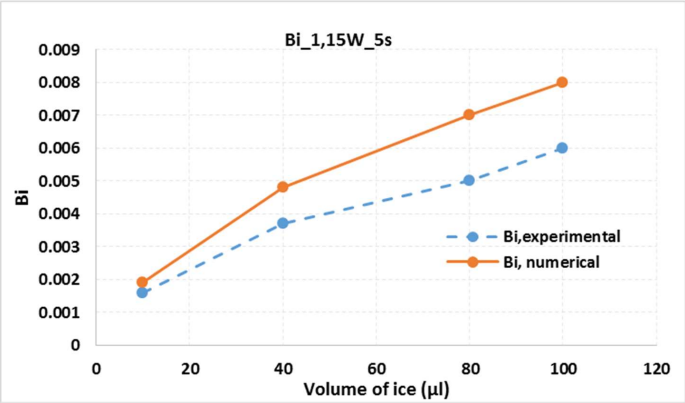

Fig.8. Biot numbers obtained for 10, 40, 80 and 100µl of ice

It shows from Fig. 8 that the Biot number is lower than 0.1 for the considered cases. This clearly implies that ~~has been done and it was lower than 0.1, inducing the fact that~~ the effect of ~~the~~ external convection~~temperature~~ on the temperature gradient of ice during the ~~releasing of~~ heat release~~ saved~~ is negligible. Thus, heat transfer dynamics achieved during this ice detection process corresponds to a lumped-heat-capacity model, neglecting convection is justified and conduction is the primary mechanism, which facilitates the use of the criterion.

~~$$B_i = \frac{h_j(V_j/A_j)}{\lambda_j} \qquad (6)$$~~

~~h_j, V_j, A_j and λ_j are respectively heat transfer coefficient around the body, volume, surface and thermal conductivity of the body.~~

Formatted: Font: Italic

Commented [U5]: Il faut réfléchir sur cela, car qu'est-ce qui se passera s'il y a des conditions de vent…

~~The Biot numbers obtained from experimental and numerical simulations for 10, 40, 80 and 100µl of ice-drop considered and positioned on thermocouple T_1 for 5s of duration of electrical pulse of 1.15W are reported on Fig.8.~~

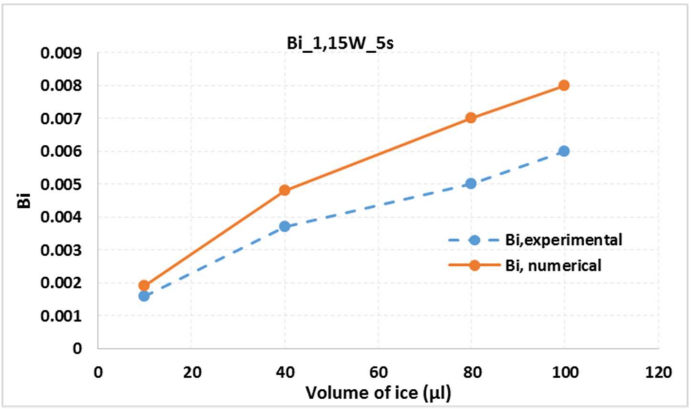

Fig.8. Biot numbers obtained for 10, 40, 80 and 100µl of ice

The effect of the electrical pulse power that is applied through the graphene sheet on the relaxation time is investigated for pulse durations of 5s. ~~For 5s of the duration of electrical pulse applied through the sheet of graphene, the effect of different electrical power of the pulse has been studied.~~ For that, we used a volume of 10µl for the ice-drops positioned ~~i~~on thermocouple T_1 and with ~~different~~ electrical powers ~~of the pulse chosen are:~~of 1.15W, 2.3W and 3.5W. The relaxation time from the numerical and experimental studies are given in Fig. 9. Given the results of Fig. 9, it appears that the relaxation times τ are practically the same~~.~~ ~~Nevertheless it appears that for the lower case of electrical power of the pulse , presence of ice can be detected slightly better than the other . For each model based on this approach of detection, it will be interesting to determine the condition in which less energy is consumed and detection of ice achieved.~~

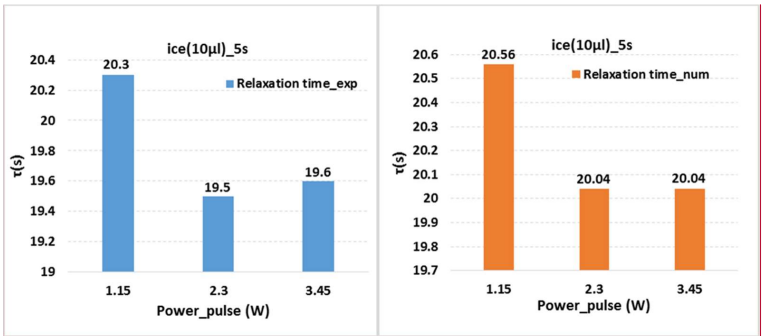

Fig.9. Relaxation time τ for different electrical power of the pulse applied to 10µl of ice-drop (a) Experimental simulation, (b) numerical simulation

Commented [U6]: Pas sûr qu'il faille le présenter comme cela. Vu l'erreur expérimentale, ces valeurs sont les même et il n'y a pas de tendance. Alors, soit il faut ajouter plus de valeur en agrandant l'échelles, soit il faut mettre ces valeurs dans un tableau.

Aussi, essayer de mettre des valeur des erreurs, avec, p.ex. des error bars.

With the advantage of good thermal properties of the sheet of graphene in the substrate, it will contribute to eliminate ice when it is detected. Moreover hydrophobic behaviour of the pre-preg helps

to reduce the energy needed for the de-icing process and gives the substrate a little icephobic character [18-19].

5. Conclusion

For each model based on this approach of detection, it will be interesting to determine the condition in which less energy is consumed and detection of ice achieved.

References

[1] N.N. Davis, Icing Impacts on Wind Energy Production, DTU Wind Energy PhD thesis (2014)
[2] L. Battisti, Wind Turbines in Cold Climates: Icing Impacts and Mitigation Systems, Green Energy and Technology Springer (2015)
[3] E. Lee, N. Karimi, H. & Krakiwsky, Road information systems: Impact of geographic information systems technology to automatic vehicle navigation and guidance, Proceedings of Vehicle Navigation and Information Systems Conference, Toronto, Canada (1989)
[4] A. Heinrich et al., Aircraft Icing Handbook, FAA Technical Center Publication, Atlantic City, NJ (1991)
[5] B. Stankov, A. Bedard, Remote sensing observations of winter aircraft icing conditions: a case study, J. Aircraft 31(1994) 79-89
[6] R.G. De Anna, M. Mehregany, S. Roy, Microfabricated ice-detection sensor, Proceedings of the Conf. Smart Struct. and MEMS, SPIE Syrup. On Smart Struct. And Mater. San Diego, CA, USA, March (1997)
[7] J. Ge, L. Ye, J. Zou, A novel fiber-optic ice sensor capable of identifying ice type accurately, Sensors and Actuators A 175 (2012) 35–42.)
[8] J.G. Mason, J.W. Strapp, P. Chow, The ice particle threat to engines inflight, in: 44th AIAA Aerospace sciences meeting and exhibit, Reno, Nevada, USA, January 9–12 (2006) AIAA2006-236,
[9] W.B. Wright, LEWICE 2.2 capabilities and thermal validation (2002) AIAA2002-0383
[10] R. Ranaudo, J. Batterson, A. Reehorst, T. Bond, T. O'Mara, Effects of horizontal tail ice on longitudinal aerodynamic derivatives, J. Air- craft 28(1989) I93-199
[11] T. Frank, A. Khodadoust, Effects of ice accretions on aircraft aerodynamics, Progress in Aerospace Sciences 37 (2001) 669–767
[12] J. Cole, W. Sand, Statistical Study of Aircraft Icing Accidents, AIAA Paper 91- 0558 (1991)
[13] X. Zhao, J.L. Rose, Ultrasonic guided wave tomography for ice detection, Ultrasonics 67(2016)212-219.
[14] E.Madi, K. Pope, W. Huang, T. Iqbal, A review of integrating ice detection and mitigation for wind turbine blades, Renewable and Sustainable Energy Reviews 103(2019)269-281
[15] T.Rashid, H.A. Khawaja, K.Edvardsen, Measuring thickness of marine ice using IR thermography, Cold Regions Sciences and Technology 158(2019)221-229
[16] N.Umair, Mughal, S.Virk, Y. Mustafa, State of the Art Review of Atmospheric Icing Sensors, Sensors & Transducers 198 (2016) 2-15
[17] T.H. Kwan, D. Ikeuchi, Q. Yao, Application of the Peltier sub-cooled trans-critical carbon dioxide heat pump system for water heating-modelling and performance analysis, Energy Conversion and Management 185(2019) 574-585.
[18] S. Xiao, J. He, Z. Zhang, Nanoscale de-icing by molecular dynamics simulation, Nanoscale 30(2016)1-8
[19] S. Xiao, J. He, Z. Zhang, Modeling nanoscale ice adhesion, Acta Mechanica Solid Sinica 30(2017)224-226

[20] S. Jung, M. Dorrestijn, D. Raps, A. Das, C. M. Megaridis, D. Poulikakos, Are Superhydrophobic Surfaces Best for Icephobicity? Langmuir 27(2011)3059-3066